Evaluation of Salt Rock Pillar Stability Utilizing Numerical Calculations, Mine Survey and In Situ Rock Mechanics Measurements

Klaus Dürr,[1] Volkmar Graefe,[1] Lutz Liedtke[2] and Dieter Meister[2]

[1]*Gesellschaft für Strahlen- und Umweltforschung mbH - München*
München and
[2]*Bundesanstalt für Geowissenschaften und Rohstoffe*
Hannover, Federal Republic of Germany

ABSTRACT

The stability of a rock salt pillar has been studied utilizing finite element calculations, measurements of deformation and acoustic emission, and mine surveying. The pillar is loaded by the pressure of the overburden and by stress redistribution from the surrounding chambers. As a result of this loading, the pillar exhibited steady-state creep. The average creep rate in the pillar is about $3 \cdot 10^{-6}\ d^{-1}$ in longitudinal direction. Creep of the rock salt pillar is accompanied by emission of high frequency acoustic energy, which has been monitored together with the pillar deformation process over a long period of time.

The finite element calculations are based on the ADINA computer code for non-linear, time-dependent problems. The creep values used for the calculations were derived from extensive laboratory experiments on rock salt.

The results of in-situ measurements have been compared with the results of the time-dependent finite element calculations and are found to be in agreement. The complete analysis of the measurements, calculations and safety assessment leads to the conclusion that, at present, the pillar is stable.

INTRODUCTION

The former Asse potash and salt mine in the Federal Republic of Germany has been operated since 1964 as a research and development facility for the solution of problems which are coupled with the safe disposal of radioactive wastes. General and specific engineering and geoscientific problems are worked on there which serve the development of methods and processes for the final disposal of radioactive wastes in geological formations. Within the scope of these investigations, low and medium radioactive wastes were deposited from 1967 until 1978. These wastes are at present still in the mine.

In view of the special use made of the R and D facility, which, due to the existing legal approval regulations, is limited at present to research projects without additional deposition of wastes, an extensive in situ monitoring program (Dürr, 1982) is being carried out with the application of the most varied methods. At the same time, the aim of making available appropriate monitoring methods for inspection of the mechanical stability of the rock of underground cavities in salt rock is being pursued.

The pillar reported on here was studied within the scope of this comprehensive program. From the example provided by it, evidence of pillar stability will be obtained on the basis of engineering-geological and geotechnical investigations and stability calculations carried out in accordance with the engineering concept for the assessment of the stability of cavities in salt (Albrecht, Meister, Stork, Wallner, 1980).

Geological Situation and Mining Conditions

The Asse mine in northern Germany is situated on an 8-km-long ridge, about 10 km SE of Wolfenbüttel. The ridge strikes from NW to SE. Its core consists of Zechstein stratigraphic sequences that were upthrust during the Upper Cretaceous (see Figures 1).

The greatly enlarged section shows that the southern flank is steeply uplifted. The northern flank has a flatter incline. In a stratigraphic assignment of the flanks in the covering rock, it follows that compared with the southern flank, the northern flank is more uplifted. The oldest stratum cropping out at the surface is the Lower Mus-

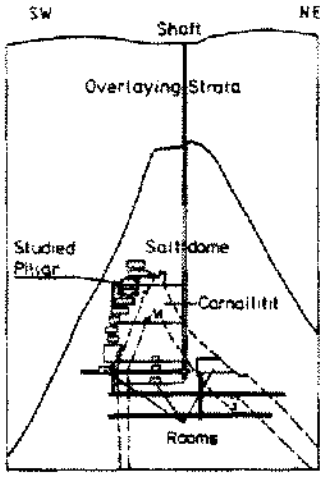

Figure 1. Cross Section South–North

chelkalk; on the northern flank it is the Lower Buntsandstein. The two slopes of the covering rock are separated by a tectonically, greatly stressed zone.

The Zechstein anticline itself is formed mainly of rock salt of the Staßfurt and Leine series. Above these, there are still strata from the youngest Aller series. Mining of the Leine rock salt took place in the southern flank from 1916 to 1965 at depths between 750 and 490 m. About 130 rooms were excavated on 13 levels (see Figure 2). They have mean dimensions of 60 m length, 40 m width and 15 m height. Normally, there are nine chambers next to each other on one level in the strike direction of the deposit. The pillar width between the chambers is 12.5 m. If there are cross-cuts or blind shafts in the pillar, this width is 20 m. Six meters were left between chambers one above the other. Mining was carried out from bottom to top. The mine was constructed using a spiral drift. The convergence of the workings is continuing. The investigated pillar is situated in this working area. Attention is drawn to the publication by Dürr, Meister (1981) for its geological structure.

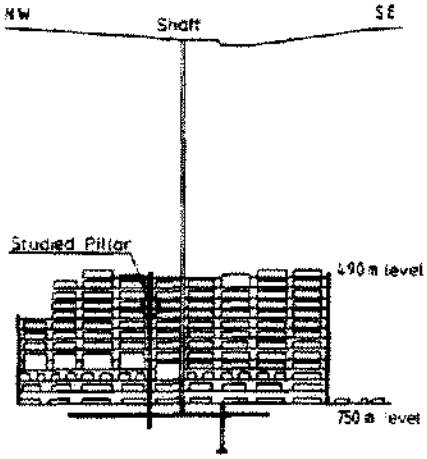

Figure 2. Cross Section West–East

A second working area is situated in the Staßfurt rock salt of the anticlinal core (see Figure 1). The chambers lie between the 775 and 725 m levels. From 1927 onward, 15 chambers of different sizes were constructed within 10 years.

On the northern flank, carnallitite was mined from the 750 m level up to a depth of 712 m. Mining was terminated in 1925. All of the cavities were backfilled.

STABILITY ANALYSIS OF A ROCK SALT PILLAR

Geometry

The pillar under study is situated at the 553 m level between chambers 4 and 5, almost in the horizontal centre of the workings. It was left standing about 1956 and thus has existed for 26 years. In the strike direction it has a width of about 20 m, whereas perpendicular to the strike it has an average length of 45 m and a height of 15 m (Figure 3). At the floor level, it is cut by a drift with a cross-section of 7 m^2, ending in the south at a blind shaft on the other side of the pillar. In addition, two entrances of the same diameter lead to the chambers on either side. An upward-running blind shaft and a former engine room of 5 m width and up to 4 m height are located on the north side of the pillar. In 1975 a spiral drift with a cross-section of 14 m^2 was opened up north of the pillar.

Numerical Calculations

FE method and ADINA code. For mathematical modelling of the investigated underground construction, the finite element method was applied, using a modified version of the ADINA computer program (Bathe, 1978).

This is a computer program for static and dynamic displacement and stress analysis of solids, structures and fluid structure systems. The program can be used for linear and nonlinear analyses. It is based on the displacement method. An isoparametric eight-noded element was used. The computation was made using the following assumptions:

- plane strain
- nonlinear, total Lagrange formulation
- Von Mises' isotropic hardening
- time increment = 10 days
- stiffness reformation and equilibrium iteration for each time step
- Poisson's ratio $\nu = 0.49$.

The general purpose computer program was expanded by a subprogram for computing the local safety factor.

Rock mechanics model and boundary conditions. The thermomechanical behaviour rock salt, considering the

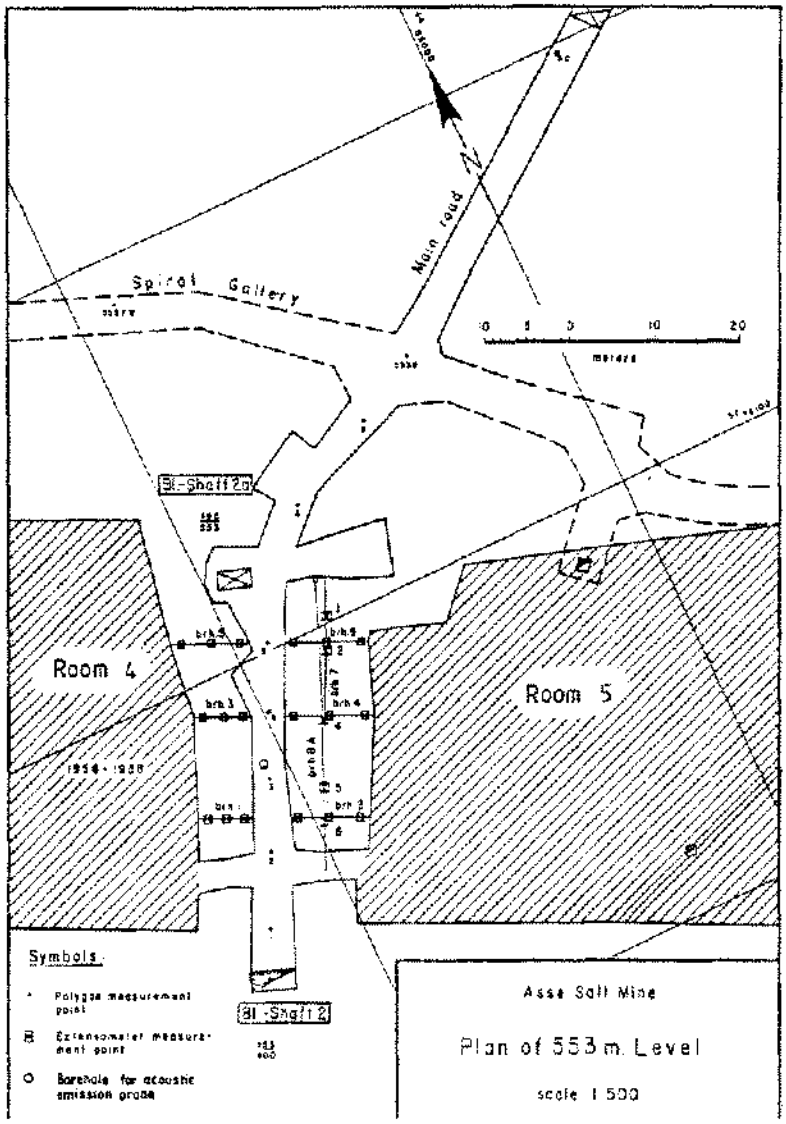

Figure 3. Measuring Layout for a Rock Salt Pillar

long term load effects, is a highly nonlinear function of time, stress and temperature. The viscous behaviour is described in general by a creep law like the Arrhenius formula, expanded by a stress term (Langer 1979):

$$\dot{\epsilon}_{\text{eff}} = A \cdot e^{-(Q/RT)} \left(\frac{\sigma_{\text{eff}}}{\sigma^*} \right)^n \qquad (1)$$

parameters:

$A = 0.18\ d^{-1}$, structure factor
$Q = 54\ MJ\ kmol^{-1}$, activation energy
$R = 8.314\ kJ\ mol^{-1}\ k^{-1}$, universal gas constant
$n = 5$, stress exponent
$\sigma = 1$ MPa, normalizing value

variables:

σ_{eff}(MPa) = effective deviatoric stress
T(K) = temperature.

The values given for the parameters are empirical values for steady-state creep of several types of rock salt.

The values used for parameters in the constitutive law for creep used for the finite element computations are subject to some uncertainty and are still being constantly improved as a result of laboratory and in-situ investigations. The following assessment of error shows the influence inaccuracies in parameters A, n and Q has on determination of the creep rate when the effective stress σ_{eff} is known.

The differential equation for the constitutive law for creep (1) is

$$d\dot{\epsilon} = \frac{\partial\dot{\epsilon}}{\partial A}\,dA + \frac{\partial\dot{\epsilon}}{\partial n}\,dn + \frac{\partial\dot{\epsilon}}{\partial\left(\frac{Q}{R}\right)}\,d\left(\frac{Q}{R}\right) \quad (2)$$

where

$$\frac{\partial\dot{\epsilon}}{\partial A} = \left(\frac{\sigma_{eff}}{\sigma^*}\right)^n e^{-(Q/RT)}$$

$$\frac{\partial\dot{\epsilon}}{\partial n} = A\left(\frac{\sigma_{eff}}{\sigma^*}\right)^n e^{-(Q/RT)} \ln\frac{\sigma_{eff}}{\sigma^*} \quad (3)$$

$$\frac{\partial\dot{\epsilon}}{\partial\left(\frac{Q}{R}\right)} = -A\left(\frac{\sigma_{eff}}{\sigma^*}\right)^n e^{-(Q/RT)}\frac{1}{T}.$$

Division of equation (2) by $\dot{\epsilon}$ and expansion of the terms on the right then gives

$$\frac{d\dot{\epsilon}}{\dot{\epsilon}} = \frac{dA}{A} + n\ln\frac{\sigma_{eff}}{\sigma^*}\frac{dn}{n} - \frac{Q}{RT}\frac{d\left(\frac{Q}{R}\right)}{Q/R} \quad (4).$$

Here, the quantities $d\dot{\epsilon}/\dot{\epsilon}$, dA/A, dn/n and $d(Q/R)/Q/R$ are the relative errors in the quantities $\dot{\epsilon}$, A, n and Q/R. (R is sufficiently well known, thus $d(Q/R)/Q/R = dQ/Q$).

As one generally does not know the sign of the relative errors, the absolute values are used and the following estimate is obtained:

$$\left|\frac{d\dot{\epsilon}}{\dot{\epsilon}}\right| \le \left|\frac{dA}{A}\right| + \left|n\ln\left(\frac{\sigma_{eff}}{\sigma^*}\right)\right|\left|\frac{dn}{n}\right| + \left|\frac{Q}{RT}\right|\left|\frac{dQ}{Q}\right|. \quad (5)$$

The relative errors in the parameters then have only a minor influence on the creep rate when their coefficients are less than 1; the constitutive law for creep is then "well conditioned". Here, however, with $\sigma_{eff} = 10$ MPa, T = 301.6 K and the previously mentioned parameter values, one obtains

$$\left|\frac{d\dot{\epsilon}}{\dot{\epsilon}}\right| \le \left|\frac{dA}{A}\right| + 11.51\left|\frac{dn}{n}\right| + 21.55\left|\frac{dQ}{Q}\right| \quad (5a)$$

i.e., the creep law in the existing form is "ill conditioned." With relative parameter errors of only 1‰, errors of 3.4% can occur in the creep rate. If one remembers that the rock stress of 10 MPa on which the finite element computation is based is an approximation, then it follows that the calculated creep rate is only qualitatively correct. Independent of the uncertainties presented, the finite element computation, nevertheless, provides a good overview of the distribution of stresses and displacements in the pillar.

The parameters for the strength behaviour of rock salt are obtained from triaxial tests with continuously loaded cylindrical samples with a diameter to length ratio of 1:2.5. It can be stated that the most important result of these tests is that rock salt can react to various stresses both with failure and also with marked visco-plastic deformations (Liedtke, Meister, 1982). The failure is clearly recognizable in the stress-strain curve as a peak point. This clearly occurs during higher rates of deformation and small lateral stresses. With increasing lateral pressure the peak point is displaced to greater amounts of strain and with higher lateral pressures it is no longer recognizable. The testing stress at 20% strain is used for determining the maximum load-bearing capacity of rock salt samples. As extensive uniaxial and triaxial tests have shown, the failure strength, or the bearing capacity of rock salt, increases with a rising strain rate up to a limiting value. This begins at a rate of deformation of about $\dot{\epsilon} = 10^{-4}\ s^{-1}$. Higher rates of deformation do not produce significant improvement of the failure strength or the load-bearing capacity.

The failure or load-bearing capacity criterion is given by the following, hyperbolic formula:

$$\tau_0 = \frac{\sigma_0 + c_0}{a_0 + b_0\cdot(\sigma_0 + c_0)} \quad (6)$$

where

$a_0 = 0.19$, initial increase of the hyperbola
$b_0 = 0.012$ 1/MPa, 1/asymptote of the hyperbola
$c_0 = 0.65$ MPa, smallest mean main stress
σ_0 = octahedral normal stress
τ_0 = " shear stress.

The octahedral normal and shear stresses are defined as follows:

$$\sigma_0 = (\sigma_1 + \sigma_2 + \sigma_3)/3$$

$$\tau_0 = \frac{1}{3}\sqrt{(\sigma_1 - \sigma_2)^2 + (\sigma_2 - \sigma_3)^2 + (\sigma_3 - \sigma_1)^2}$$

$\sigma_2 = \sigma_3$ (in the case of the triaxial tests).

Equation 6 applies for strain rates of $\dot{\epsilon} = 10^{-4}\ s^{-1}$

The summary in Figure 4 is exemplary for all Brazilian uniaxial and triaxial test results of a test series with Asse rock salt. The normal deviation amounts to $\sigma_{\tau 0} = \pm 1.3$ MPa. This τ_0/σ_0 diagram in combination with the finite element computations serves for assessment of the stress reserves.

If the computed values lie above the values in Figure 4, then failure or unacceptedly high rates of deformation must be taken into account in the construction concerned. A possible local safety factor can be defined as follows:

$$\eta = \frac{\tau_0 \text{ available (according to equation (6))}}{\tau_0 \text{ possible (according to FE computations)}} \quad (7).$$

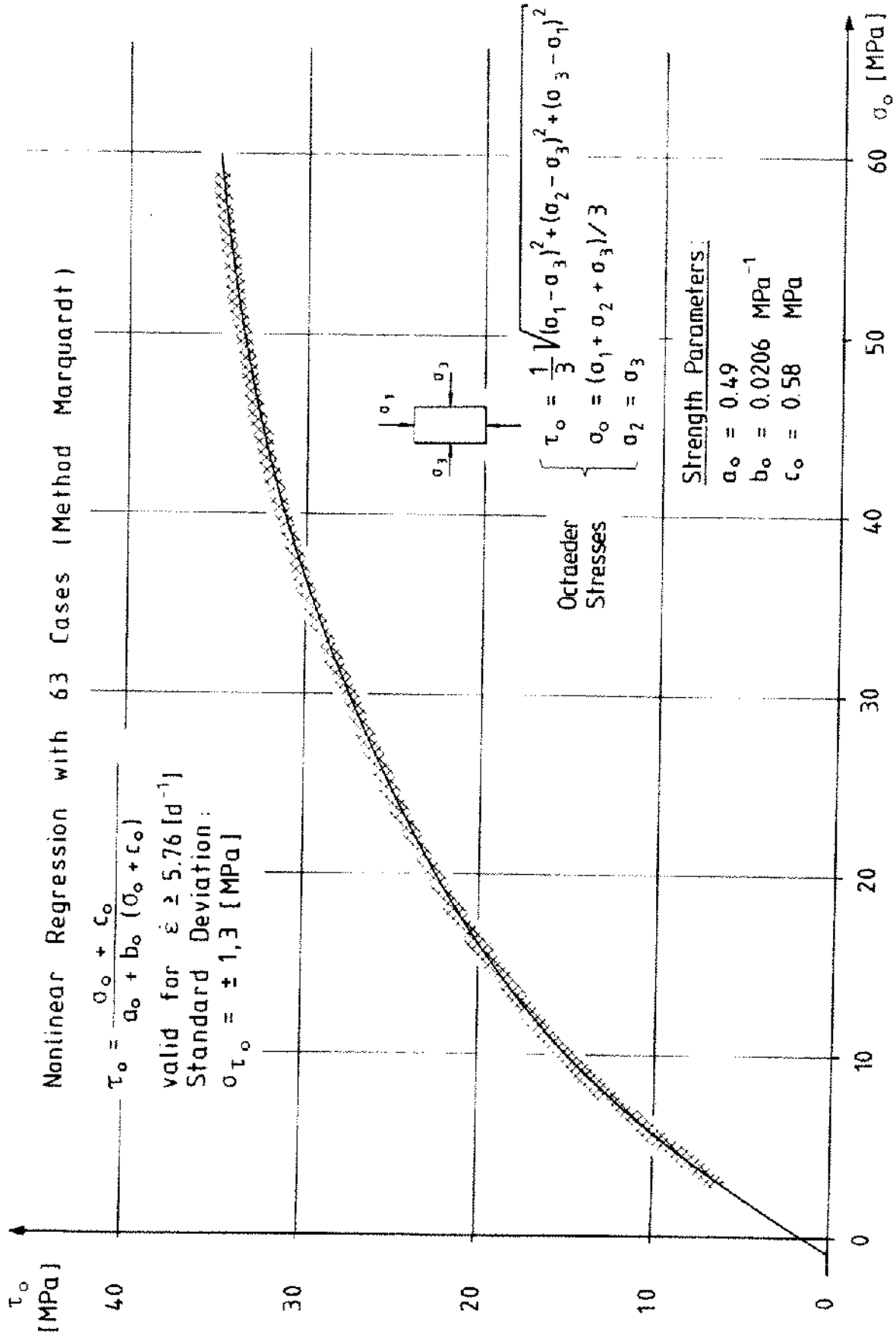

Figure 4. Load Bearing Capacity Diagram, Asse Rock Salt (Na2)

Investigated load case. A horizontal section was selected for the computation that roughly characterized the middle of the pillar (Figure 5). Here, the one side of the pillar is held constant and the position of the other is variable.

For the numerical model, a pressure of 10 MPa was assumed as realistic. With the geometrical boundary conditions described previously, together with the rock salt constitutive law for creep, the failure criterion, the load distribution and the mesh shown in Figure 6, the nonlinear stress-deformation as a function of time was then calculated.

Technical Measurement Investigations

Mine survey measurements. The measuring layout for the pillar is shown in Figure 3. In the main drift, polygon points are indicated for measuring the pillar longitudinal displacements. The points are steel rods of 1.5 m length. They are installed in boreholes in the roof of the drift. The upper 10 cm of the rod are cemented into the rock. The measurements of the distance between points are made at half-yearly intervals with precise surveyor's tapes and since 1981, by using electro optical length measurement techniques. For this purpose, a high-precision electronic tachymeter (Elta 2) made by Zeiss (Oberkochen) was used. The corrections resulting from measuring tape calibration, temperature effects and atmospheric conditions are included in all measurement results.

The accuracy of the linear measurements made since 1962 differs according to which measuring instruments was used:

tape measurement 1962–1966: ± 1 mm
1966–1981: ± 0.5 mm,
electro-optical distance measurement 1981–1982 with application of the polar method: ± 1.5 mm.

The analysis of these measurements was made without the use of electronic data processing. The results are plotted normally in displacement-time graphs.

Extensometer measurements. Three extensometer reference points were installed in each of the boreholes 1 to 6 to monitor the transverse expansion of the pillar. These are wire extensometers that are anchored in the rock with expansion shell bolts. The wires lead to measurement studs in the main drift. The points lie in an approximately horizontal plane about 1 m above the floor level. They are installed in such a way that they are at a distance of 1 m from the outer surface of the pillar as well as from the wall of the main drift. This distance was chosen after a hook sounding of the boreholes in order to keep the influence of the near-surface flaking effects on the measurement to a minimum. The third point in each borehole is situated in the middle between the other two anchored points. The measuring points are checked manually every three months with mechanical instruments.

In addition to the points in the boreholes, horizontal drift convergence is observed by means of two extensometer studs opposite one another. As systematic investigations have shown, the measurement accuracy for the determination of changes in length is about 0.05 mm.

Rod extensometers were installed in boreholes 7 and 8a, in the eastern half of the pillar at points 1 to 3 and 4 to 6, respectively (Figure 3). The level of the points in borehole 8a is almost the same as the plane of the transverse strain reference points. Borehole 7, however, was drilled slightly uphill. The measuring points are therefore located 1 to 2 m above the comparison plane. The two extensometer measurement locations are equipped with a long-term data acquisition system with the object of continuously obtaining information on the pillar deformation and to correlate this with simultaneously registered acoustic emission measurements. The extensometer rods are connected to inductive displacement pickups in measurement heads on the wall. The output signals are read by a PCM data acquisition system and are registered on magnetic tape above ground.

An important factor in the accuracy of measurement at the rod extensometer is the tolerance of the displacement pickups used. Depending on the measuring range, lengths of between 50 and 150 mm and tolerances of ± 0.2 to ± 0.3 mm were determined by calibration measurements for the maximum test values. As only a part of the measuring range has been used, the error in the measurements is only a sixth of that given above. Errors due to the data acquisition system range from only ± 0.025 mm to ± 0.075 mm because of the high resolution of the system (2.4 mV) at the maximum value of 5 V. Combining these two sources of error, the error in determining length changes is at worst ± 0.1 mm, at measurement points far from the measuring heads. The inaccuracy for measurement points near the measuring heads is about 50% less. The effect of errors associated with temperature variations in the vicinity of the pillar can be disregarded. Long-term temperature measurements confirm this. Since 1977, an average air temperature of 301.6 K has been monitored in the drift.

Microacoustic measurements. Pillar deformation in both horizontal dimensions is caused by creep and is accompanied by the emission of acoustic energy resulting from the formation and development of fissures and effects associated with the creep mechanism. It was assumed that in the case of steady-state pillar creep the emission of acoustic energy is statistically constant. This had to be proved by measurement.

The microacoustic emission of the rock pillar was monitored using a single-channel prototype system, which is presently undergoing further development.

The borehole for acoustic emission measurements was drilled downward from the floor of the pillar drift in the middle of the pillar (Figure 3). The monitoring station is

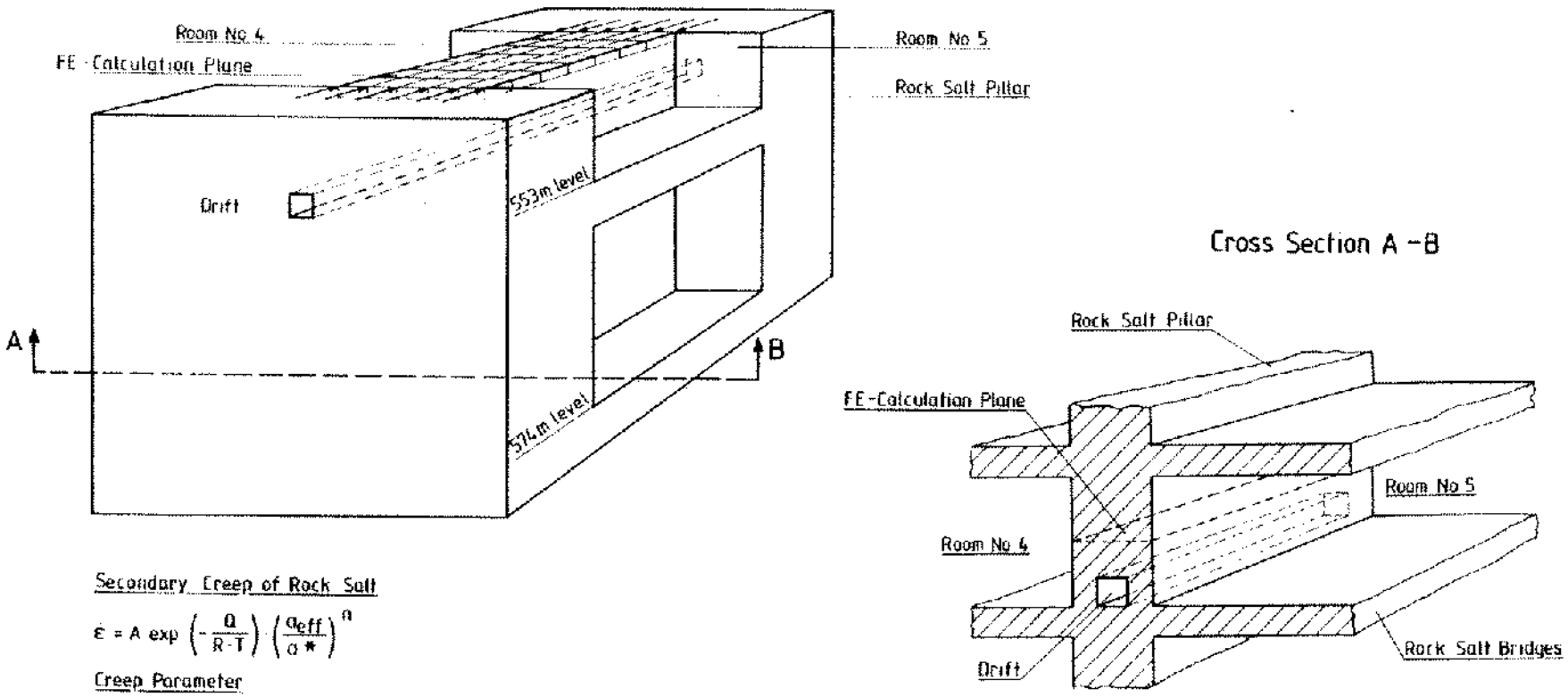

Secondary Creep of Rock Salt

$$\dot{\varepsilon} = A \exp\left(-\frac{Q}{R \cdot T}\right) \left(\frac{\sigma_{eff}}{\sigma^*}\right)^n$$

Creep Parameter

$A = 0.18 \quad d^{-1}$
$Q = 54 \quad MJ \cdot k\,mol^{-1}$
$\sigma^* = 1\ MPa$
$n = 5$
$R = 8.314\ kJ \cdot k\,mol^{-1}\,K^{-1}$
$T = 301.6\ K$

Elastic Material Parameter

$E = 25000\ MPa$
$\nu = 0.49$

Figure 5. Geomechanical Model

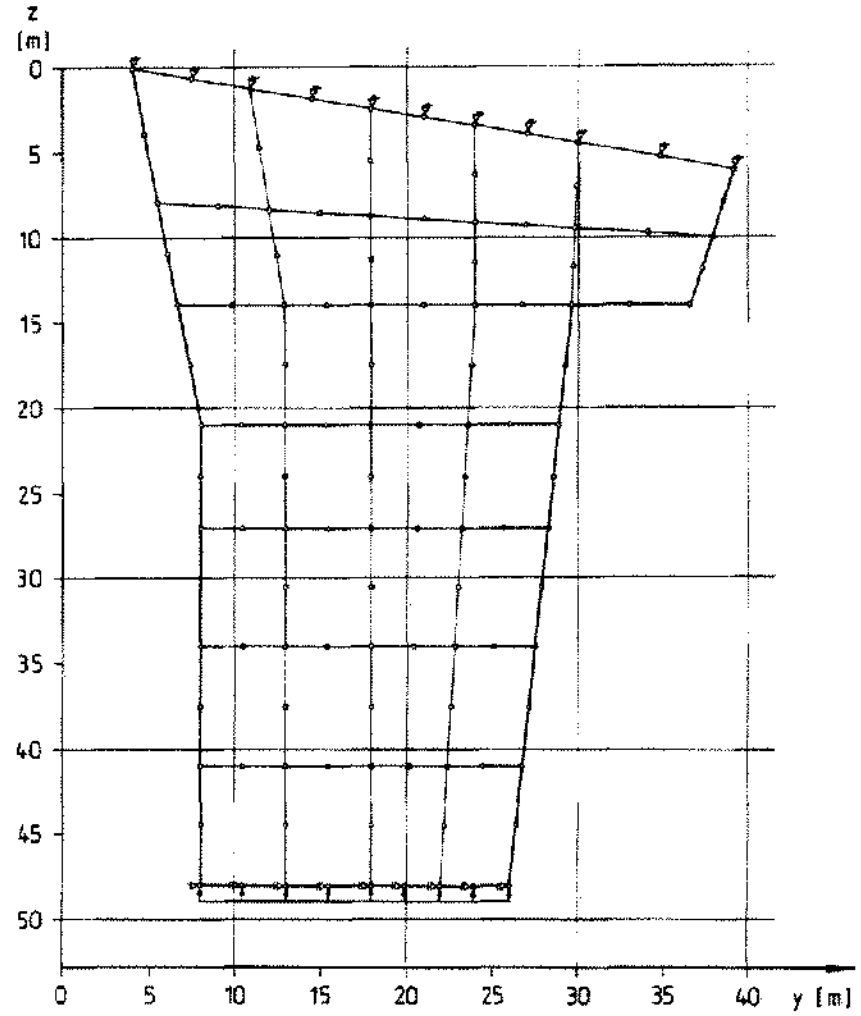

Figure 6. Finite Element Mesh for Stability Analysis

about 25 m from the borehole. The probe was placed at a depth of 3 m and fastened to the rock salt by pressing the sharp end of the probe into the bottom of the borehole.

A piezoelectrical crystal serving as an acoustic transducer was installed in a borehole probe, together with a preamplifier with a gain of 40 dB noise voltage of about 10μV. Resonance frequencies of the transducer occur between 13 and 15 kHz and above 90 kHz.

The analysis of the acoustic emission measurements concentrated on two aspects:

a) long-term counting of events
b) distribution of magnitude of signal amplitudes.

Acoustic events are continuously monitored. For analysing the signal amplitudes, the acoustic emission signals are recorded on magnetic tape or stored on floppy discs. The stored signals are played back in the laboratory. Magnetic tape records were taken at about one-year intervals.

The event rate per hour R_h is calculated for analysing the frequency of events using

$$R_s = \frac{N}{\Delta t}$$

$$R_h = \sum_{i=1}^{36} \left(\frac{N}{\Delta t} \right)_i$$

where

N = number of events
Δt = 100 s = integrating time
R_s = event rate during a period of 100 s
R_h = event rate during a period of 1 hour.

The cumulative frequency of events can be calculated for further information. The results of this analysis give a very good overview of the variation in event rate with time.

The main point of the studies is the analysis of the dis-

tribution of amplitudes. It is well known from geophysical literature that the seismic activity of a certain area can be described by the following law (Karnik, 1964; Leydecker, 1975; Tsumura, 1967):

$$\log N_k = \alpha - \beta M \tag{9}$$

where

N_k = cumulative frequency of magnitudes
M = magnitude of seismic event
α, β = empirical parameters.

The question has been raised as to whether their equation is also valid for acoustic emission phenomena caused by rock salt pillar creep. According to the laboratory investigations of hard rock by Scholz (1968), very good correlation with seismic field measurements can be confirmed. He found that the parameter β is mainly influenced by the stress in the rock. Therefore, emphasis has been placed on analysis of this parameter.

Investigation Results

Finite element computations. The calculation of stresses and deformations was carried out with the previously mentioned assumptions (FE method and ADINA code) for a period of 900 days. No significant changes in stress could be determined within this period. The largest stresses of $\sigma_{zz} = 10$ MPa on the narrow side of the pillar decrease on the wider side to $\sigma_{zz} = 2 - 7$ MPa. The complete distribution of stress is shown in Figure 7. In the same figure, the creep-producing effective stress σ_{eff} for two sections A-A and B-B are shown. In most of the pillar area they were determined to be between 7 and 8.5 MPa.

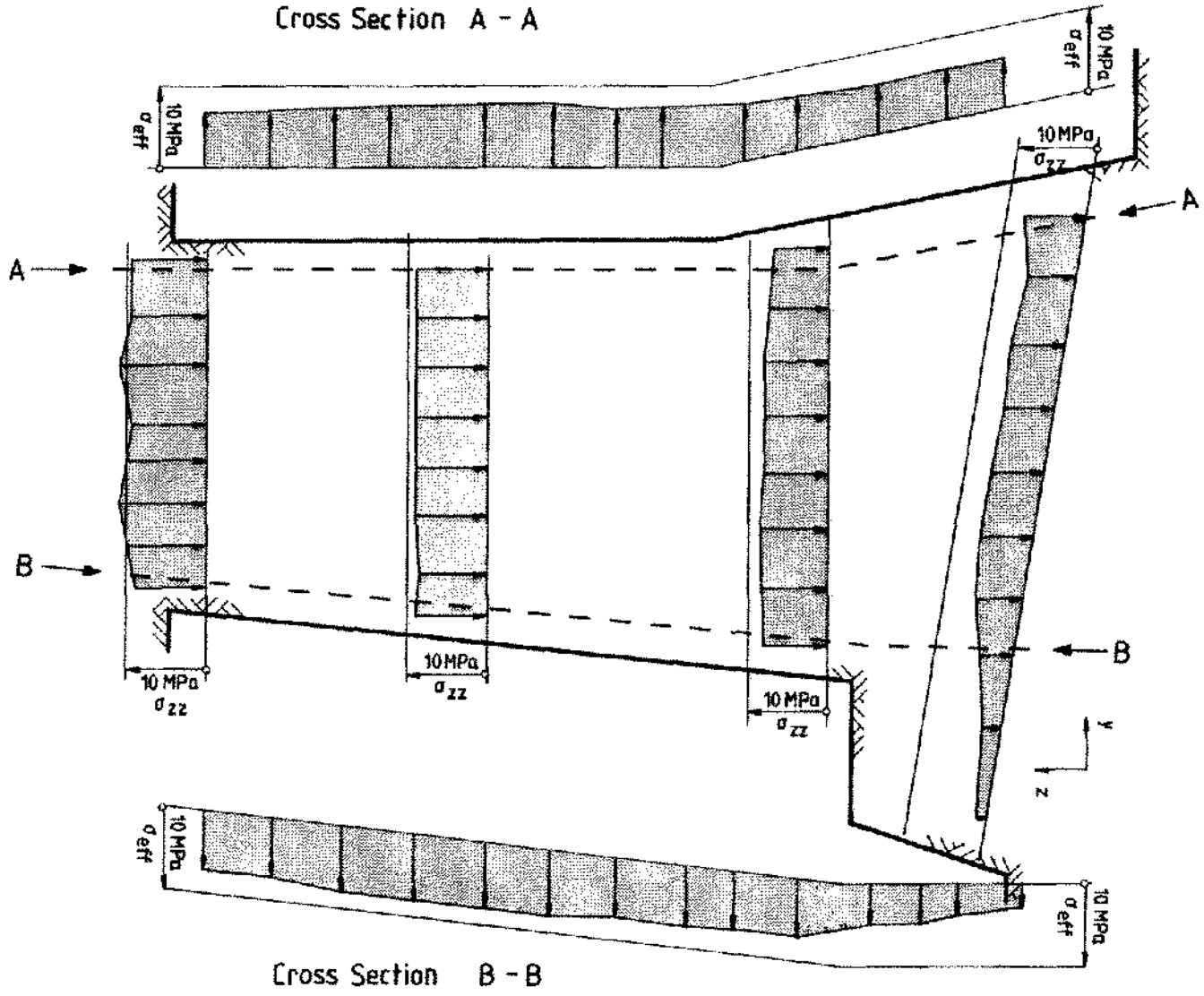

Figure 7. Distribution of Stresses σ_{zz} and σ_{eff}

The displacements associated with the stress shown are plotted in Figure 8 for the total period of 900 days. During the plotting of the displacements, the zero point of the coordinate system was placed at the pillar centre. Apart from the compression of the pillar in the z-dimension, the bulging out in the y-dimension is clearly recognizable. The measured and computed lateral displacements for two extensometer pairs (Ext. No. 3–4 and 5–6) in the y-dimension are demonstrated in Figure 12. The fact that the curves are nearly parallel indicates good agreement between computed and measured results. It can be seen that the computed results are slightly greater than the observed ones. This is also true for the curves in Figure 10, in which the displacements in the z-dimension are compared for polygon points 3 and 4. These points are roughly at the middle of the pillar and have a distance of about 8 m from each other.

A comparison of the computed stresses with the maximum permissible stresses (equation 7) enabled a statement on the local safety factors to be made. The lines connecting points with equal safety factors (isoasphalic lines) provide an overview of the distribution of safety fac-

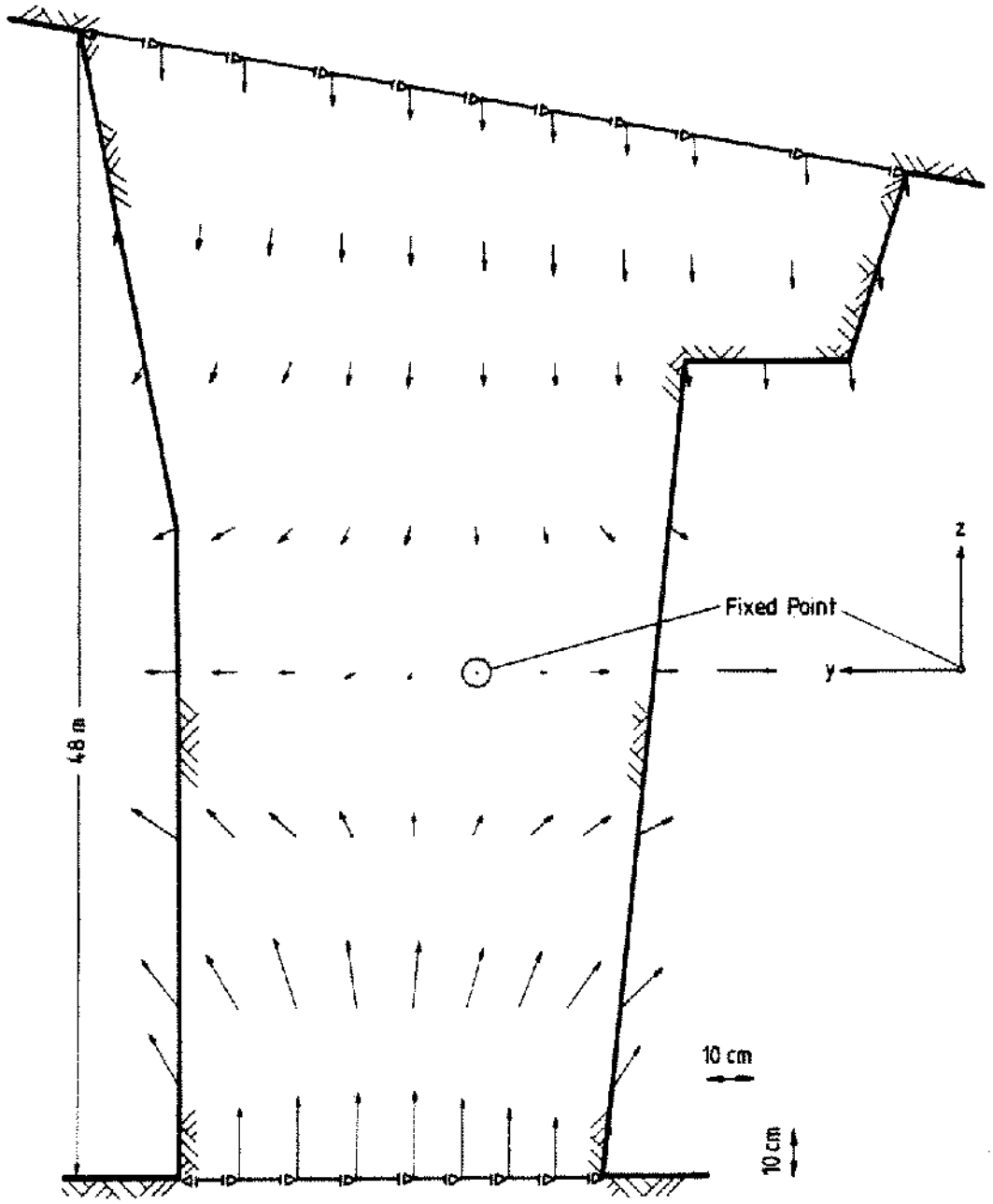

Figure 8. Displacements after 2.5 Years

tors (Figure 9). These isoasphalic lines are plotted for the last time increment.

At the northern and southern boundaries of the pillar, the local safety factor of $\eta \geq 3$ is greater than in the central area, where it falls to a still satisfactory value of $\eta = 1.9$.

Measurements. 1. *Deformations.* Figure 10 shows the results of pillar compression measurements over a period of 20 years. The changes in distance between polygon points 3 to 4 are shown as an example. These points were selected to permit a simultaneous comparison with the computer studies. The displacement curve is linear during the entire period of measurement. From this, it can be derived that the pillar is in a state of steady-state creep (Langer, 1979) between polygon points 3 and 4. The long-term, mean creep rate for this pillar area is $3.5 \cdot 10^{-6}$ d^{-1}. The results of the pillar displacement measurements using the two rod extensometers No. 7 and No. 8a (Figure 3) confirm the longitudinal measurements in the parallel pillar stage. The mean creep rate measured between anchors 1 to 6 over a period of 3.65 years amounts to $3.1 \cdot 10^{-6}$ d^{-1}.

It can be seen in Figure 11 that the pillar compression is not evenly distributed along the pillar axis. The displacements measured between the individual polygon points are plotted in this figure for the time since measurements were begun in 1962. As the displacement measurements in the pillar drift were carried out in the crosscut as far as shaft 2 on the north side of the pillar, the area between the pillar and shaft 2 could also be monitored. It is therefore clear from Figure 11 that the pillar area between polygon points 1 and B is compressed. An expansion zone adjoins in the northern abutment of the pillar.

The pillar transverse deformations determined in several measurement planes (Figure 3) using a rod extensometer are shown in Figure 12. Depending on the location of these measurement planes, various large transverse displacements are recognizable which, like the pillar compressions, increase linearly with time. The largest transverse deformation occurs at the middle of the pillar (Ext. 3 and 4). The creep rate here is $5.2 \cdot 10^{-6}$ d^{-1} and is thus greater than the creep rate of the pillar compression measured in the long term between polygon points 3 and 4. Creep rates of $2.9 \cdot 10^{-6}$ d^{-1}, or $0.1 \cdot 10^{-6}$ d^{-1} were measured in the off-centre transverse displacement mea-

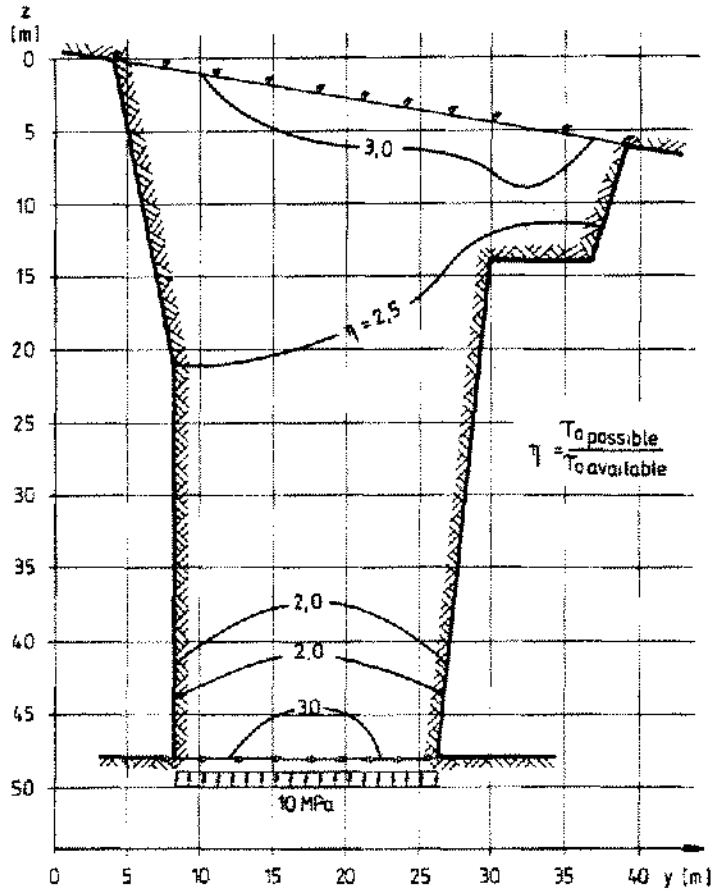

Figure 9. Isoasphalic Lines

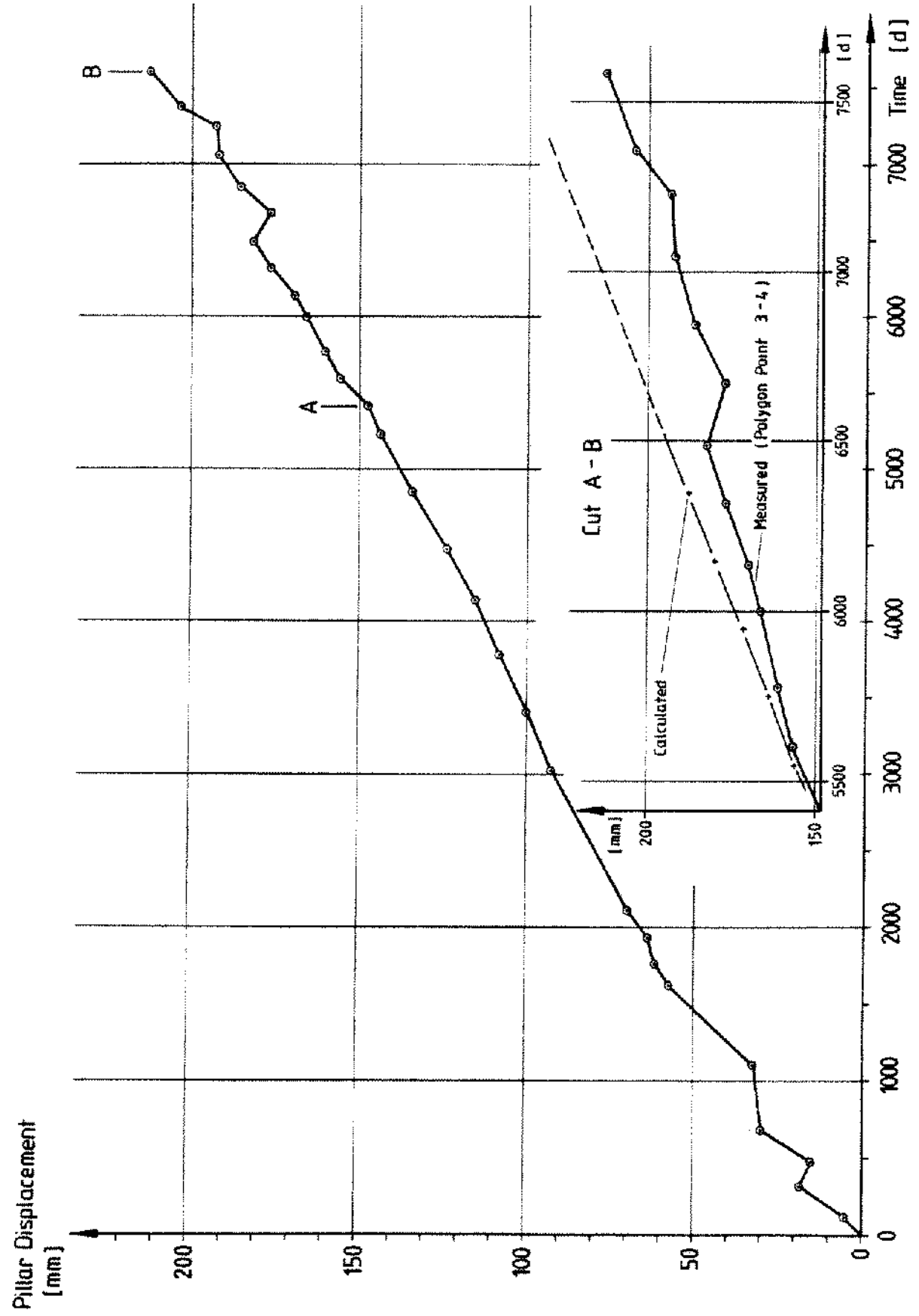

Figure 10. Measured and Calculated Pillar Displacement between Polygon Points 3 and 4

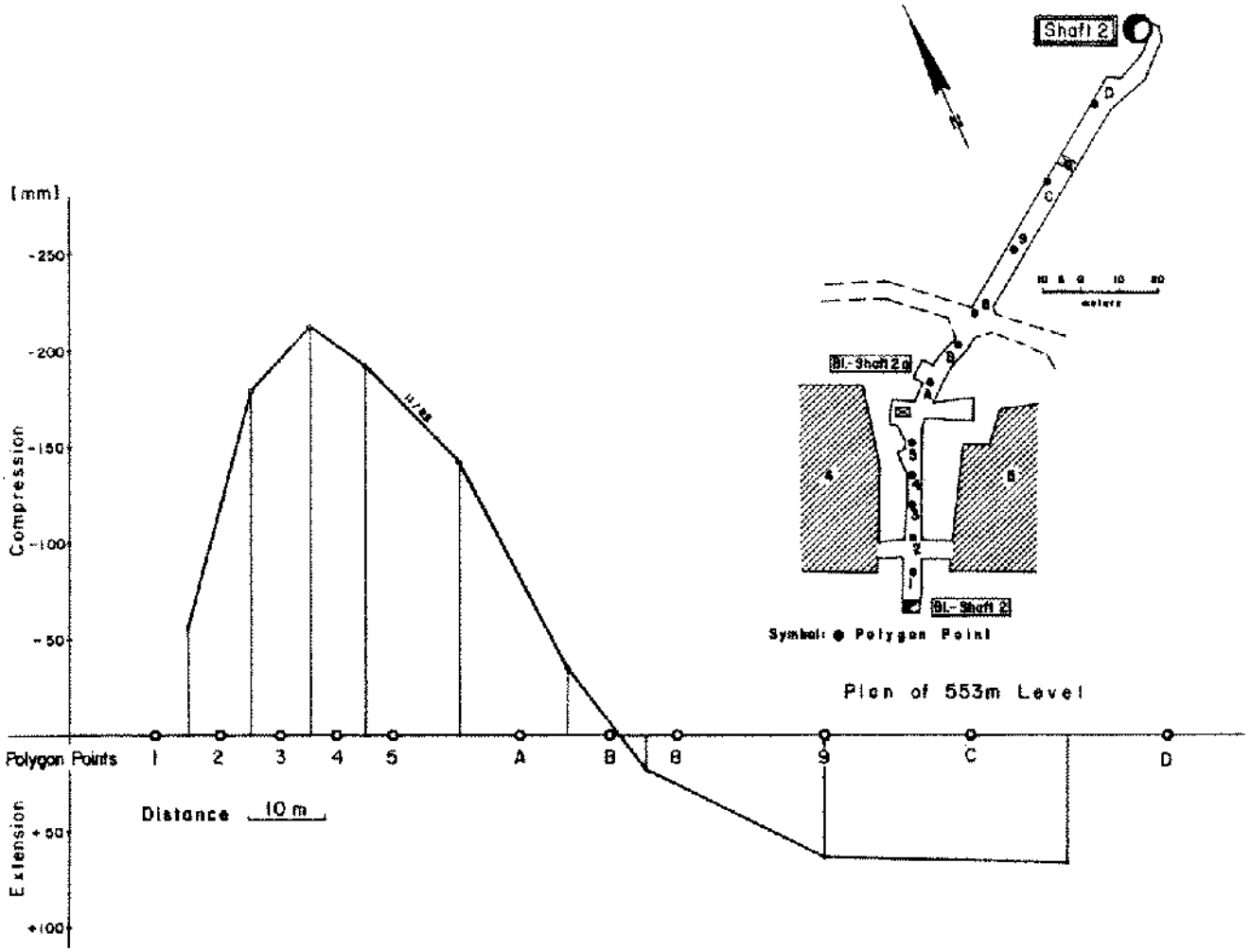

Figure 11. Distribution of Polygon Points Displacement

surement cross-sections (Ext. 5 and 6 as well as 1 and 2). All of the measurements were made during a period of 5.62 years.

2. *Acoustic emission measurements.* As can be seen in Figure 13, the acoustic emission rate varies quite distinctly during the period under consideration. Mining noise has been eliminated in the plot, thus the measured events are thought to be acoustic energy emitted as a result of longitudinal and transverse deformation of the rock salt pillar. Figure 13 shows that the emission rate curve is not a very regular one but is characterized by many peaks appearing over a period of several days. The reason for this behaviour is that the acoustic emission transducer receives signals from all over the pillar, from the more highly stressed interior part and from partly destressed parts close to the surfaces of the adjacent chambers or the pillar drift. As a result, it can be stated that event rate and pillar deformation do not correspond.

The main objective of the acoustic emission studies is the distribution of amplitudes. As an example, Figure 14 shows the results of four magnetic tape recorders. Starting with formula (9) the following equation was obtained:

$$\log f(A/A_0) = a - 20b \log(A/A_0) \qquad (10)$$

where

$f(A/A_0)$ = cumulative frequency of pulses of a given amplitude
A_0 = amplitude, set at 6 dB above noise level
A = measured amplitude
a, b = empirical parameters.

Parameters a and b, the coefficient of correlation R, and the average values of the event rate are summarized in tabular form in Figure 15. As can be seen, no significant variation is noted for the b-value, over a period of 2.5 years. The constant b-values are in accordance with the constant creep rates for the pillar deformation. Whether this is accidental has to be established by future measurements.

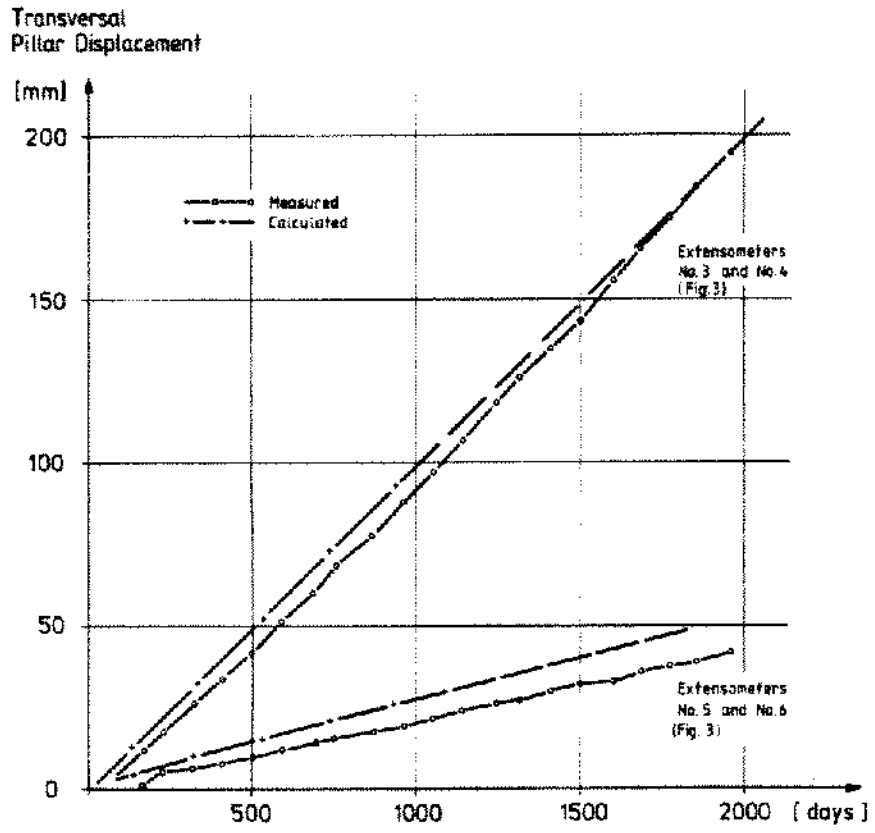

Figure 12. Comparison between Measured and Calculated Transversal Pillar Displacements

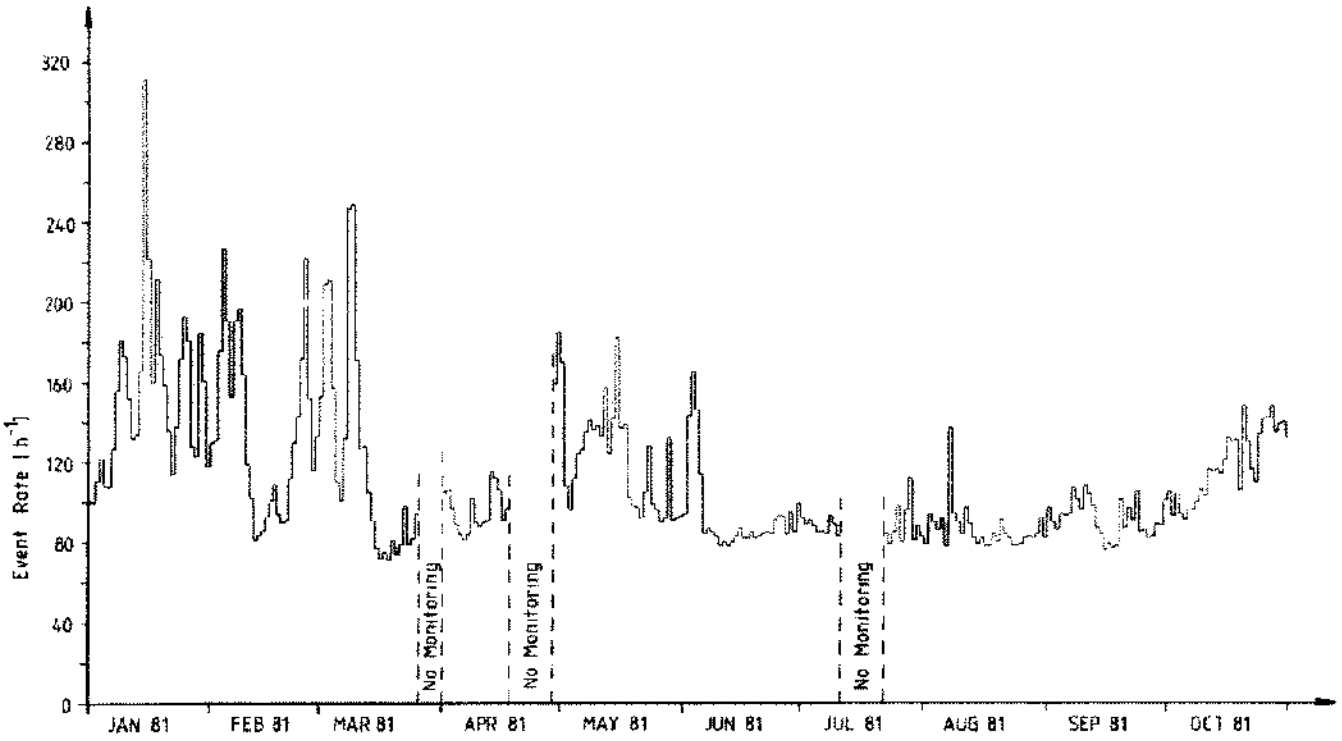

Figure 13. Acoustic Emission Rate

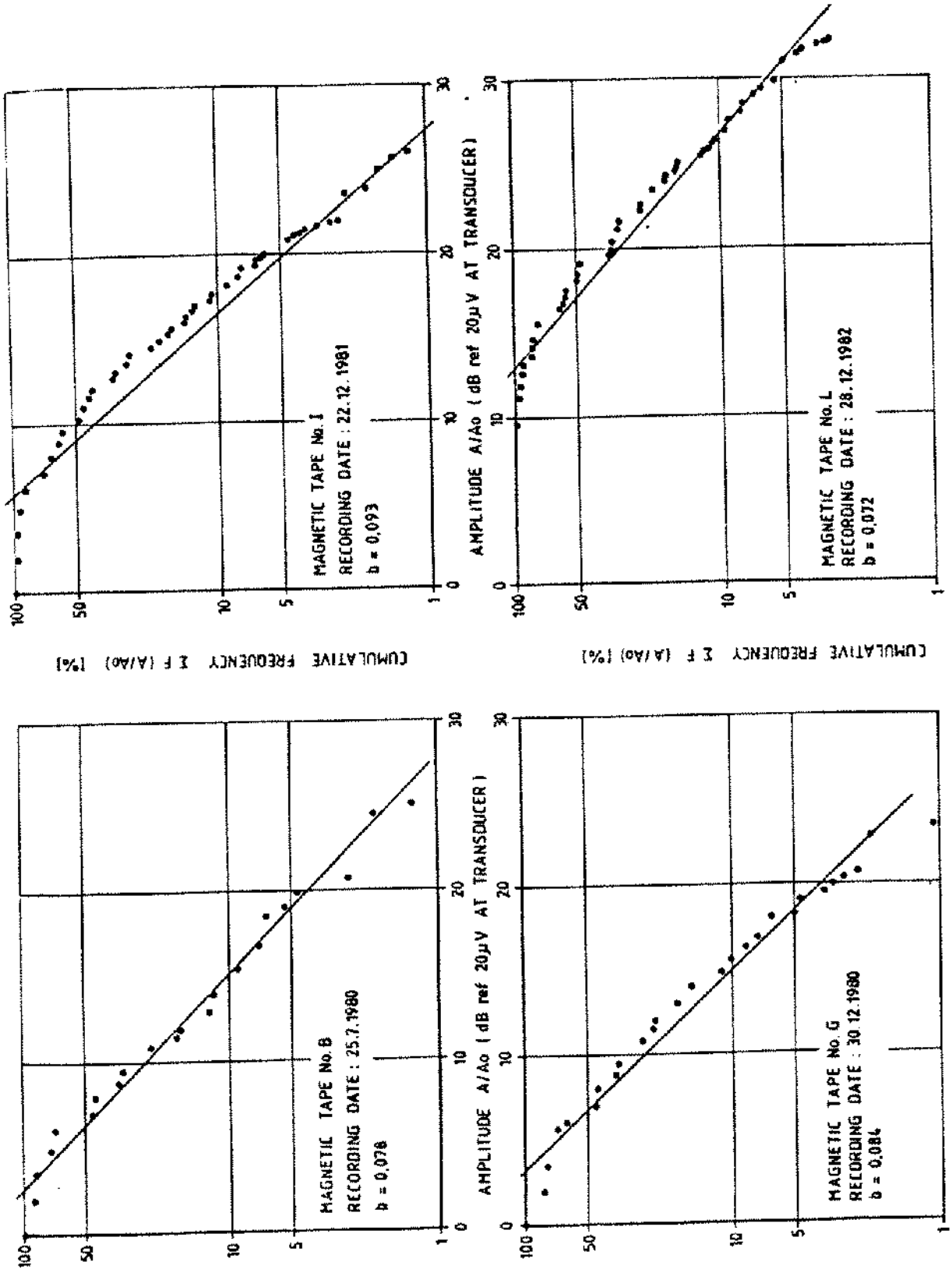

Figure 14. Cumulative Frequencies of Maximum AE-Amplitudes versus Amplitude

RECORDING DATE	MAGNETIC TAPE No.	EVENT RATE [min^{-1}]	COEFFICIENTS OF FREQUENCY DISTRIBUTION b	a	REGRESSION COEFFICIENT R	NUMBER OF EVENTS N
7.25.1980	A 1	2,7	0,1134	2,3946	0,968	79
"	A 2	2,3	0,0830	2,1727	0,973	64
"	A 1+2	2,5	0,0970	2,2308	0,954	143
7.25.1980	B 1	2,5	0,0616	2,0927	0,931	74
"	B 2	2,6	0,0993	2,2263	0,981	75
"	B 1+2	2,6	0,0781	2,1900	0,990	149
7.25.1980	C 1	2,3	0,0714	2,1450	0,950	69
"	C 2	2,6	0,0794	2,4010	0,987	74
"	C 1+2	2,5	0,0816	2,3109	0,986	143
8. 1.1980	D 1	3,3	0,1043	2,5061	0,909	96
"	D 2	3,2	0,0943	2,3142	0,968	92
"	D 1+2	3,2	0,0981	2,3399	0,979	188
12.30.1980	G 1	5,0	0,0866	2,0326	0,985	142
"	G 2	4,6	0,0897	2,5538	0,984	135
"	G 1+2	4,8	0,0842	2,2608	0,982	277
12.22.1981	I 1+2	7,6	0,0929	2,5554	0,961	411
12.22.1981	K 1+2	6,4	0,0925	2,5070	0,960	374
12.28.1982	L 1+2	7,9	0,0716	2,9362	0,987	440

Figure 15. Coefficients of Amplitude Frequency Distribution

ASSESSMENT OF RESULTS OF MEASUREMENTS AND CALCULATIONS

On the basis of numerical calculations using a simple geomechanical model, long-term deformation measurements, and acoustic emission measurements over a period of several years, it is possible to assess the bearing capacity of the observed pillars from the engineering point of view. In the process, one must consider that the planes for the calculated and observed displacements are not identical (Figure 5). The vertical pillar section shows that a triaxial state of stress in the intersection of the horizontal support system and the pillar is present. This leads to a considerable hindrance of transverse deformation of the pillar in this area. As the displacement measurements could not be carried out at the level of the computation plane for mining technology reasons, then apart from the possibility of a better interpretation of the measurement results, the computations provide an important supplement to the assessment of the pillar stability and make it possible to determine deformations in the central area of the pillar, which are not influenced by bridges.

Slight differences between deformation measurements and computation results are mostly traceable to the arrangement of the measuring points (extensometer anchors) near the surfaces of the pillar, which are affected by flaking off (sheeting), or near the surfaces of drifts, the margins of which undergo a relaxation of stress.

From both the available results of the deformation and acoustic emission measurements and the computations carried out, it can be concluded that the stability of the pillar is assured at the present time. This statement is supported by the following findings:

- The pillar creep rate has been constant for 20 years and is significantly less than that in uniaxial laboratory tests which resulted in a creep failure.
- The horizontal pillar stresses are of the order of 10 MPa or less. They are relatively evenly distributed over the pillar width and do not alter significantly with time. The effective deviatoric stress causes creep increases from the wider to the narrower side; however, it does not reach values greater than 8 MPa. Creep failure is thus not to be expected.
- After 3 years of observation of the acoustic emission, no significant change in the b-value for the amplitude distribution was established.
- The visual observation of the pillar provided no indications of impending pillar failure.

This study of the stability of a single rock salt pillar must be viewed in terms of its significance to the stability

of the whole complex of 13 levels of galleries on the SW flank of the Asse anticline. When this large configuration of underground workings is considered, the following conclusions were drawn from the investigations:

1. A hypothetical creep failure of a single pillar does not imply the loss of stability throughout the mine. Instead the entire support system around the chambers must be considered as a whole.
2. The supporting system of all the chambers can explain the fact that the pillar horizontal support system is less stressed than would be expected from the overburden pressure. Computations for the mine as a whole and in situ measurements would make it possible to check the bearing capacity of the rock salt structure.

Due to the special use of the Asse mine as an R and D facility for the final disposal of radioactive wastes of the Federal Republic of Germany, the continuation of these investigations is of great importance. The intention is to proceed by stages, taking into consideration rock structures of ever increasing size, up to simulations of the entire support system for the underground workings on the SW flank. In addition to the measurements already described, rock stress measurements, measurements with vertically installed extensometers, ultrasonic and temperature measurements at fixed points are to be carried out. It is also intended to continue the computer investigations, with consideration of spatial support effects and larger sections of rock.

ACKNOWLEDGMENTS

This research work was done thanks to the provision of financial support from the Minister for Research and Technology, Federal Republic of Germany.

REFERENCES

Albrecht, H., D. Meister, G.-H. Stork and M. Wallner, 1978. Zur Frage des Standsicherheitsnachweises von Hohlräumen in Salzgesteinen. Proc. 5th Int. Symp. on Salt, Hamburg, V. I, pp. 195–211, Cleveland, Ohio.

Bathe, K.-J. 1978. A finite element program for automatic dynamic incremental nonlinear analysis, MIT, Cambridge, Mass.

Dürr, K. 1982. Deformationsmessungen zur Beurteilung der Standsicherheit in einem ehemaligen Salzbergwerk. V. Internationales Symposium für Markscheidewesen, 19.–26. September 1982, Varna, Bulgarien, Band 4.

Dürr, K. and D. Meister, 1981. Evaluation of pillar stability in a salt mine, utilizing acoustic emission, mine survey and rock deformation data. Third Conf. on Acoustic Emission/Microseismic Activity in Geologic Structures and Materials, October 5–7., Pennsylvania State University, University Park, Pa.

Karnik, V. 1964. Magnitude frequency relation and seismic activity in different regions of Europe. Bull. Int. Inst. Seism. Earthquake Eng., V. I. 9–32.

Langer, M., 1979. Rheological behaviour of rock masses, Proc. 4th Int. Congr. on Rock Mechanics, Montreux, V. III, pp. 29–96.

Leydecker, G., 1975. Seismizitätsstudien im Bereich des Peloponnes auf Grund von Präzisionsherdbestimmungen.-Dissertation, Universität Frankfurt/Main.

Liedtke, L. and D. Meister, 1982. Stability analysis of underground structures in rock salt utilizing laboratory and in-situ testing and numerical calculations. Solution Mining Research Institute Meeting, October 3–6, Manchester, England.

Scholz, C. H., 1968. The frequency-magnitude relation of microfracturing and its relation to earthquakes.-Bull. Seism. Soc. Am. V 58. 399–417.

Tsumara, K. (1967): Determination of earthquake magnitude from total duration of oscillation. Bull. Earthquake Res. Inst., V 45, pp. 7–18.